Author postprint
Published in J. Magn. Magn. Mater. 268 (2004) 364-373

Title :
Effects of silicon addition on the electrical and magnetic properties of copper-doped (La,Ca)MnO_3 compounds

Authors :
B. VERTRUYEN[1*]
A. RULMONT[1]
R. CLOOTS[1]
M. AUSLOOS[2]
J.-F. FAGNARD[3]
S. DORBOLO[3]
Ph. VANDERBEMDEN[3]

[1] LCIS, Chemistry Institute B6, Sart Tilman, University of Liège, B-4000 Liège, Belgium
[2] SUPRAS, Physics Institute B5, Sart-Tilman, University of Liège, B-4000 Liège, Belgium
[3] MIEL, Montefiore Institute B28, Sart Tilman, University of Liège, B-4000 Liège, Belgium

* corresponding author :
e-mail : b.vertruyen@ulg.ac.be, phone : + 32 4 3663452, fax : + 32 4 3663413

ABSTRACT

In this paper we report about the electrical properties of $La_{0.7}Ca_{0.3}MnO_3$ compounds substituted by copper on the manganese site and/or deliberately contaminated by SiO_2 in the reactant mixture. Several phenomena have been observed and discussed. SiO_2 addition leads to the formation of an apatite-like secondary phase that affects the electrical conduction through the percolation of the charge carriers. On the other hand, depending on the relative amounts of copper and silicon, the temperature dependence of the electrical resistivity can be noticeably modified : our results enable us to compare the effects of crystallographic vacancies on the A and B sites of the perovskite with the influence of the copper ions substituted on the manganese site. The most original result occurs for the compounds with a small ratio Si/Cu, which display double-peaked resistivity vs. temperature curves.

PACS numbers : 75.30.Vn ; 71.30.+h ; 61.72.Mm

Keywords : manganates, perovskite, electrical resistivity, grain boundaries

1. Introduction

Since the early nineties, there has been a renewed interest for the mixed-valence manganates $Ln_{1-x}A_xMnO_3$ (where Ln is a lanthanide cation and A is often an alkaline earth ion), due to the discovery of their colossal magnetoresistance (CMR) [1,2]. On one hand, films [3] of these materials could have potential applications, e.g. as magnetic sensors or in computer memory systems [4]. On the other hand, it was expected that the understanding of the underlying physical mechanisms could lead to substantial advances in the field of strongly correlated electrons physics. It rapidly turned out that the manganate system is in fact extremely complex : a wide variety of properties can be observed, depending on relatively small changes in chemical composition [5]. In the "usual" CMR compounds (whose $La_{0.7}Ca_{0.3}MnO_3$ is probably the most famous example), a maximum in magnetoresistance is coupled to a transition in both the electrical and magnetic properties, i.e. from a ferromagnetic/metallic-like phase at low temperature to a paramagnetic/insulating phase at higher temperature. But manganate compounds can also display various antiferromagnetic orders [6], orbital [7] or charge [8] ordering, spin glass properties [9], phase-separated ground states [10], …

The "double exchange" model proposed by C. Zener in the fifties [11] was first used in order to explain qualitatively the properties of the classical CMR compounds. Manganate compounds crystallize in ABO_3 perovskite-related structures. The B ion (here Mn) is surrounded by 6 oxygen ions and the degeneracy of the d orbitals is removed. The main idea of the Zener model is that the electrical conduction happens through hopping of e_g electrons without spin-flip. Since those electrons are strongly coupled (by the Hund rule) to the t_{2g} core spins, the resistivity is drastically decreased in case of parallel alignment of the core spins, i.e. in the ferromagnetic state or when a magnetic field is applied (magnetoresistance effect). Unfortunately, the Zener model fails to yield reliable quantitative – and sometimes even qualitative - predictions. However, it has been experimentally proved that the parameters used in this model are valid [12] : the physical properties are influenced by the Mn^{4+}/Mn^{3+} ratio, also called "charge carrier density", and by the crystallographic structure (especially the Mn-O distances and Mn-O-Mn angles) which affects the properties by modifying the orbital overlapping and thus the transfer integral. It was indeed experimentally observed that the transition temperature varies with the mean A site radius $\langle r_A \rangle$ [13,14] and the size mismatch σ^2_A [15,16].

In order to probe the exact role of the Mn-O network, various substitutions on the Mn site were also studied, generally with a transition metal as doping cation : Cr, Fe, Co, Ni, Cu, Ru,… [17-20]. The case of copper doping was examined with a particular interest due to the major role played by copper in the high-T_c superconductors. Indeed the first papers on copper doping dealt with $La_{1-x}Ba_xMn_{1-y}Cu_yO_3$ [21,22], because of the similarity with the superconductor $La_{2-x}Ba_xCuO_4$. Cu doping was also studied in the case of $LaMnO_3$ [23-24], $La_{1-x}Sr_xMnO_3$ [25] and more recently $La_{0.7}Ca_{0.3}MnO_3$ [26-28]. Initially we were interested in copper substitution on the manganese site of $La_{0.7}Ca_{0.3}MnO_3$. The idea to add silica results from an accidental contamination of the first batch of samples during the grinding in an agate mortar : some of these samples displayed double-peaked features in their resistivity vs. temperature curve. Therefore we decided to study the electrical properties of $La_{0.7}Ca_{0.3}MnO_3$ compounds substituted by copper on the manganese site and deliberately contaminated by SiO_2 in the reactant mixture. Obviously, it was also necessary to study the "reference" series, i.e. (i) silica-contaminated $La_{0.7}Ca_{0.3}MnO_3$ compounds and (ii) copper-doped $La_{0.7}Ca_{0.3}MnO_3$ compounds. As mentioned above, other authors had already studied the copper-doped compounds [26-28], but we had to synthesize this series as well since the values of electrical resistivity and transition temperature vary as a function of the synthesis conditions.

2. Experimental

A set of samples with nominal molar composition "$La_{0.7}Ca_{0.3}Mn_{1-x}Cu_xO_3$ + y SiO_2" (where x = 0.04 and y = 0.02, 0.04, 0.08 ; or x = 0.08 and y = 0.04) was prepared by a standard solid state reaction method. Two series of reference compounds were also synthesized following the same procedure : $La_{0.7}Ca_{0.3}Mn_{1-x}Cu_xO_3$ samples with x = 0.02, 0.04, 0.06 and "$La_{0.7}Ca_{0.3}MnO_3$ + y SiO_2" samples with y = 0, 0.04 and 0.08. Proper amounts of lanthanum oxide (La_2O_3), calcium carbonate ($CaCO_3$), manganese oxalate ($MnC_2O_4.2H_2O$), copper oxide (CuO) and silicon dioxide (SiO_2) were thoroughly ground in petroleum ether and heated to 1200°C with intermediate grindings. Pellets were pressed uniaxially and fired to 1300°C for 48 h. Compositions and labels are collected in table I.

X-ray diffraction patterns were recorded with a Siemens D5000 diffractometer (CuK_α radiations). The cell parameters were refined in the Pbnm space group with the Fullprof software. The microstructural properties were characterized by scanning electron microscopy (Philips XL30 ESEM) and optical microscopy with polarized light (Olympus AH3-UMA). The cationic composition was checked by energy dispersive X-ray analysis (EDX) coupled to the electron microscope.

The physical properties measurements were carried out using a Physical Property Measurement System from Quantum Design. Resistivity measurements were performed with the standard four-probe method. The magnetic behavior was studied by AC susceptibility measurements at 1053 Hz under 1mT and by DC magnetic moment measurements.

3. Results

Typical X-ray patterns are displayed in figure 1, one for each series of samples. The manganate peaks are marked by a star (*). A secondary phase (peaks marked by a cross (+)) is observed in every silicon-containing sample. These crystallographic reflections are similar to those of the lanthanum calcium silicate $CaLa_4(SiO_4)_3O$ phase (JCPDS 71-1368). The cell parameters of the manganate phase were determined by Rietveld refinement. In the $La_{0.7}Ca_{0.3}Mn_{1-x}Cu_xO_3$ series, Cu doping up to 6 % does not lead to a significant variation of the lattice parameters. In the "$La_{0.7}Ca_{0.3}Mn_{1-x}Cu_xO_3$ + y SiO_2" series, no significant variation of the peak positions and widths is observed. In the "$La_{0.7}Ca_{0.3}MnO_3$ + y SiO_2" series, a small (0.01 Å) but significant increase of the cell parameters of the manganate phase is detected when the silica content is increased from 4 to 8 %.

Electron microscopy on fractured samples shows a typical grain size of about 5-10 microns, without excessive porosity or variance in grain size. Microscopic and EDX characterizations of polished cross-sections indicate that $La_{0.7}Ca_{0.3}Mn_{1-x}Cu_xO_3$ samples are homogeneous. On the contrary, the presence of a secondary phase was confirmed in the silicon-containing samples. This phase contains silicon (found only in this phase), oxygen, lanthanum, calcium and copper (when present). No manganese was detected in the secondary phase. The EDX results confirm that the ratio "A-site cations/B-site cations" in the manganate phase decreases as the silicon content increases. In the samples C4S4 and C4S8, copper is found only in the silicate phase. (Note that the 2 % copper in C2S0 could be detected by EDX, so a possible residual copper amount in the manganate phase of C4S4 and C4S8 would be less than 2 %). In samples C4S2 and C8S4, copper is found in both the silicate and the manganate phases. A few Mn_3O_4 grains were observed in most samples.

The electrical resistivity vs. temperature curves of the $La_{0.7}Ca_{0.3}Mn_{1-x}Cu_xO_3$ samples are shown in figure 2. Each sample undergoes a "metal-insulator" transition. The peak temperature T_p decreases and the maximum resistivity increases as the copper content x increases. Figure 3 shows the temperature dependence of the electrical resistivity of the Cu-

free samples C0S0, C0S4 and C0S8. The peak temperatures are almost equal but the resistivity increases with the silicon content. The resistivity of the samples containing both silicon and copper is presented in figures 4 and 5. The C4S4 and C4S8 samples (figure 4) display only one peak in their resistivity behavior, with almost identical peak temperature. The resistivity increases with the silicon content. The C4S2 and C8S4 samples (figure 5) present a double peak behavior. The C8S4 sample is more resistive than the C4S2 sample. The peak temperatures of each sample are reported in table I. Magnetoresistance curves (not shown here) mimic the resistance curves, with one or two peaks at temperatures corresponding to the resistive transitions. It should be noted that the low temperature peaks of the C4S2 and C8S4 samples behave similarly to the usual I-M transition peaks : they are significantly shifted to higher temperatures under application of a magnetic field.

A few representative AC susceptibility curves are shown in figure 6 : respectively for a Cu-free sample (C0S8), for a Si-free sample (C4S0), for a “single peak” sample (C4S8) and for a “double peak” sample (C8S4). They are typical of a paramagnetic-to-ferromagnetic transition. The transition temperatures T_c (defined as the intersection of the tangent to the inflexion point of the m’(T) curve with the abscissa axis) are reported in table I. Additional magnetic characterization was performed on the C4S2 and C8S4 samples. The results are shown in the case of the C8S4 sample. Figure 7 displays the temperature dependence of the AC magnetic susceptibility (1 mT, 1053 Hz) with superimposed DC magnetic fields ranging from 0.1 T to 1 T. Figure 8 shows the temperature dependence of the DC magnetic moment under DC fields lying between 0.01 T and 1 T.

4. Discussion

4.1. "$La_{0.7}Ca_{0.3}MnO_3$ + y SiO_2" series

The X-ray diffraction and EDX analysis results indicate that silicon does not enter into the manganate perovskite phase but transforms upon heating into a silicate phase containing only silicon, lanthanum, calcium and oxygen. The X-ray pattern is very similar to that of $CaLa_4(SiO_4)_3O$, a silicate with apatite-type structure. Horita *et al.* [29] obtained similar results when studying the reaction between calcium-doped lanthanum chromite and silica. Besides they noticed that the fusion of this silicate phase occurs only at about 1500°C, so it is likely that there is no melted phase in our 1300°C-treated samples.

Since in the initial mixture the amounts of La, Ca and Mn were in stoechiometric proportions, the uptake of some calcium and lanthanum into the silicate phase leads to the creation of vacancies on the A site of the ABO_3 perovskite structure, as confirmed by the EDX results. The manganese in excess in the manganate phase could have been released by formation of manganese oxide grains, but only a few Mn_3O_4 grains were found during the microscopic characterizations. This confirms that the manganate phase of the C0S4 and C0S8 samples is cation-deficient on the A site.

It appears that the physical properties are not drastically altered by the consequences of the addition of SiO_2 ($y \leq 0.08$). The fact that the resistivity increases with the Si content is likely to be due to the insulating nature of the silicate secondary phase leading to a lengthening of the percolation path of the charge carriers. The temperatures T_p and T_c of the transitions are almost identical in C0S4 and C0S8. This seems to indicate that the two main parameters that influence the transition temperature (i.e. the Mn-O-Mn geometry and the Mn^{4+}/Mn^{3+} ratio) are not strongly altered by the cation deficiency on the A-site. Indeed it appears from X-ray diffraction patterns that the modification of the crystallographic structure is small : therefore the orbital overlapping is probably not strongly modified. Concerning the

Mn^{4+}/Mn^{3+} ratio, it can be noted from the phase diagram [5] that, around 30% Mn^{4+}, the transition temperature is not very sensitive to variations of the Mn^{4+}/Mn^{3+} ratio. Besides, another explanation can be put forward, based on a very interesting study of Dabrowski *et al.* [30] : these authors observed that $La_{1-x}Ca_xMnO_3$ samples prepared with constant experimental conditions (temperature and atmosphere of the thermal treatment) display an almost constant Mn^{4+}/Mn^{3+} ratio, irrespective of the chemical composition for a rather large composition range. This might be the case for our samples too, since all our samples were prepared with the same thermal treatment. Finally, the constant value for T_p in C0S4 and C0S8, though unexpected, is not so surprising. It is interesting to notice that the influence of A-site vacancies depends strongly on the type of material : for example, the introduction of vacancies on the A site of $LaMnO_{3.00}$ creates Mn^{4+} species and drastically alters the physical properties, since the antiferromagnetic insulating compound becomes ferromagnetic and metallic due to the creation of Mn^{4+}/Mn^{3+} double exchange interactions [31,32].

4.2. $La_{0.7}Ca_{0.3}Mn_{1-x}Cu_xO_3$ series

The substitution of manganese by copper leads to a rapid decrease of the transition temperatures T_p and T_c. The magnetic and electric transitions are still present for a 6 % doping. Results from the literature [26,27] indicate that the transitions eventually disappear for further doping. The introduction of a foreign cation in the manganese-oxygen network obviously disturbs the double exchange mechanism and creates scattering sites for the charge carriers. Similar phenomena were observed for several other transition metal doping cations (Fe, Co, Cr, Ni,…) [17-20]. Copper is generally considered to enter the perovskite structure as a Cu^{2+} cation. To our knowledge, this was not definitely proved in the case of manganate compounds but experimental evidence was provided for similar perovskite materials [24,33], and most authors make this assumption [17,23,24,34].

Several possibilities have to be examined concerning the local interactions of a Cu^{2+} ion with the surrounding Mn^{3+} and Mn^{4+} ions. From the electrical charge point of view, it is likely that the density of Mn^{4+} is higher in the immediate neighborhood of Cu^{2+} in order to maintain charge neutrality on the local scale. The exchange interactions also have to be considered. Cu^{2+} (d^9) is a Jahn-Teller ion, like Mn^{3+} (d^4). However the orbital ordering driven by the Jahn-Teller effect that is observed in $LaMnO_3$ is destroyed in $La_{0.7}Ca_{0.3}MnO_3$ by the large amount of Mn^{4+} ions [35]. Since no significant evolution of the crystallographic structure is observed upon Cu doping up to 6 %, it is likely that Orbital Ordering (OO), if any, would be confined to clusters around the Cu^{2+} ions. In order to illustrate the complexity of the system we have applied the Goodenough-Kanamori rules of superexchange [36,37] to different possible virtual transfers (see figure 9) :

(i) $Mn^{3+} + Cu^{2+} \Leftrightarrow Mn^{4+} + Cu^{+}$: considering a virtual electron transfer from the Mn^{3+} half-filled e_g orbital to the half-filled Cu^{2+} e_g orbital, the superexchange interaction would be antiferromagnetic.

(ii) $Mn^{3+} + Cu^{2+} \Leftrightarrow Mn^{2+} + Cu^{3+}$: a virtual electron transfer from the half-filled Cu^{2+} e_g orbital to the empty Mn^{3+} e_g orbital would be ferromagnetic, but the virtual electron transfer from the filled Cu^{2+} e_g orbital to the empty Mn^{3+} e_g orbital would be antiferromagnetic.

(iii) $Mn^{4+} + Cu^{2+} \Leftrightarrow Mn^{3+} + Cu^{3+}$: a virtual electron transfer from the Cu^{2+} half-filled e_g orbital to an empty Mn^{4+} e_g orbital would be ferromagnetic, but the virtual electron transfer from the Cu^{2+} filled e_g orbital to an empty Mn^{4+} e_g orbital would be antiferromagnetic.

(iv) $Cu^{2+} + Cu^{2+} \Leftrightarrow Cu^{3+} + Cu^{+}$: a virtual electron transfer from a Cu^{2+} half-filled e_g orbital to a Cu^{2+} half-filled e_g orbital would be antiferromagnetic.

In the previous analysis, both high-spin and low-spin states of Cu^{3+} have been considered, but it must be stressed that the low-spin singlet state is more likely in case of distortion of the CuO_6 octahedron. Without detailed investigations by local probes of the magnetic structure around the Cu^{2+} ions, no firm conclusion can be drawn. However it appears clearly that the Cu^{2+} ions are not simple "punctual" defects but that their influence extends to a larger neighborhood, introducing antiferromagnetic interactions and magnetic frustration in small clusters.

4.3. "$La_{0.7}Ca_{0.3}Mn_{1-x}Cu_xO_3$ + y SiO_2" series

Similarly to what happens in the "$La_{0.7}Ca_{0.3}MnO_3$ + y SiO_2" samples, the silica reacts during the thermal treatment and forms a silicate phase with lanthanum, calcium and (in this case) copper. In the case of the C4S4 and C4S8 samples, all the copper seems to be trapped in the silicate phase. Those samples are insulating and paramagnetic at high temperature and become both metallic and ferromagnetic at a temperature of 245 K. This transition temperature is significantly lower than that of the C0S4 and C0S8 samples (256 K), indicating that the copper departure leaves vacancies on the manganese site, in addition to the A site vacancies created by the lanthanum and calcium ions trapped in the silicate phase. If a complete "recombination" of the A and B site vacancies occurred, the resulting manganate phase should have the same transition temperature as the Cu-free compounds C0S4 and C0S8. Besides, the fact that the C4S4 and C4S8 samples display the same transition temperature despite different silicon contents confirms that the key factor affecting the T_p decrease is the concentration of Mn site vacancies. However such a decrease in transition temperature due to the Mn site vacancies is much less pronounced than that due to the substitution by Cu^{2+} on the Mn site. The fact that the Cu^{2+} ions are much more deleterious to the conduction process indicates that a Mn site vacancy has a smaller influence on the physical properties : maybe due to a smaller spatial extent of the perturbation and/or a less severe modification of the interactions. Indeed a Mn-site vacancy disrupts the manganese-oxygen network, but does not create antiferromagnetic interactions. A vacancy in the crystallographic structure does not prevent the ferromagnetic alignment of the remaining Mn ions spins. It is interesting to note once again that the consequence of such vacancies is much more drastic in the case of $LaMnO_{3.00}$, where it creates Mn^{4+} ions and leads to the appearance of double exchange, ferromagnetism and electrical conductivity [38].

Unlike the C4S4 and C4S8 samples, the C4S2 and C8S4 samples present a double peaked temperature dependence of the resistivity. This has to be related to the most noticeable difference between the two groups of samples : in the C4S2 and C8S4 samples, copper is found not only in the silicate phase but also in the manganate phase. This is not the first time that resistive double peaks are reported in the manganate-related literature. We have to confront our results to earlier published data in order to find out the cause of the double peak behavior of our samples.

- Double peaks are often observed in the resistance curves of samples prepared at low temperature by precursors methods [39,40]. Those materials are generally characterized by a small grain size. But the micrographies of our samples prove that this is not the case here.
- A double peak is also observed in the case [41] of samples post-annealed in low oxygen partial pressure, where the grain-boundary regions become oxygen-deficient. On the contrary our samples were prepared in air, what is known to yield oxygen-stoichiometric materials [30].

- Other authors [42] deliberately used a mixture of $La(OH)_3$ and La_2O_3 as source of lanthanum and obtained double peaks. But our La_2O_3 was calcined before use.

The common point of all these observations is that those double peak samples are by some way inhomogeneous : difference between core and shell of the grains in the first two cases, macroscopic inhomogeneity in the third one.

The C8S4 and C4S2 samples are of course inhomogeneous due to the presence of the silicate secondary phase, but this is the case for every Si-containing sample, having or not a double peak behaviour of the resistivity. Therefore there must be an additional inhomogeneity in the manganate phase itself. Let us consider that the system contains two manganate phases with different transition temperatures (labelled LT-phase and HT-phase). A double peak behaviour of the resistivity will occur if the current has to cross both types of regions when passing through the sample. The system can be roughly viewed as a network of two kinds of resistors placed in series and in parallel. Although the current always percolates through the less resistance path, the peaks of the two phases are expected to appear in the global resistance curve. When the temperature is increased, the metal-insulator transition of the LT-phase first occurs, resulting in the low-temperature peak of the global resistivity curve. On increasing the temperature further, the transition of the HT-phase is reached, which is responsible for the high temperature peak.

At this stage, we have to take into account that the AC magnetic susceptibility displays only one transition. Magnetic moment measurements were carried out under several fields (figure 8) and several DC fields were superimposed on the AC field in the AC susceptibility measurements (figure 7) in order to reveal any other transition. Despite this thorough investigation, only one transition could be detected, at a temperature close to the resistive transition of the HT-phase. Therefore the LT-phase must have a very small volume fraction. The fact that this minority phase has a significant impact on the resistive properties indicates that the current has to cross it and cannot percolate through a HT-phase-only conductive path. It is thus likely that the LT-phase is located at the grain boundaries : this is the most "efficient" place for a phase of small volume fraction to affect the electrical conduction.

We have now to examine the nature of the HT- and LT-phases. The EDX analysis has shown the presence of copper ions in the manganate phase but the sensitivity and accuracy of our system are not sufficient to analyse small variations inside the grains. Nevertheless, relevant information can be obtained by comparing the transition temperatures of the different samples. The temperature of the high-temperature resistive transition of C4S2 is almost equal to the transition temperature in C4S4 and C4S8. The same holds true for the magnetic transition. Therefore it is very likely that the HT-phase is in fact a Cu-depleted manganate phase similar to the manganate phase of the C4S4 and C4S8 samples. As a consequence, the copper ions detected by EDX must principally be contained in the LT-phase. This is confirmed by comparing the temperature of the low-temperature resistive transition of C4S2 with the transition temperature of the C4S0 sample : the difference is less than 20 K.

Finally, the analysis of these results is in accordance with a model constituted by a Cu-depleted majority phase and a Cu-containing minority phase located at the grain boundaries. It is worth emphasizing that double peaks appear in the compounds where there is a relatively smaller amount of silicate phase compared to the copper doping. It seems that in the case of those samples, all copper ions could not be trapped into the silicate phase (for our experimental synthesis conditions) and that the remaining copper ions are preferentially located at the grain boundaries. It is likely that the system is still out of equilibrium from the point of view of the copper distribution between the silicate and manganate phase. The presence of copper near the grain boundaries can be related to an easier diffusion at the grain boundaries than within the bulk [41].

5. Conclusion

In summary, we have confirmed the key role of the manganese-oxygen network in the physics of manganate compounds, especially in the electrical and magnetic properties. The transition temperatures are decreased when copper ions are substituted on the manganese site. Copper ions have a more pronounced influence than simple manganese site vacancies due to the antiferromagnetic superexchange interactions of Cu^{2+}.
The effect of the addition of SiO_2 in the reactant mixture was also studied. It appears that silicon does not enter the perovskite phase but reacts during the thermal treatment to yield an apatite-type phase containing lanthanum, calcium, silicon, oxygen and copper when present. In the "$La_{0.7}Ca_{0.3}MnO_3$ + y SiO_2" samples, the addition of a small amount of SiO_2 leads to A-site vacancies which do no alter very much the physical properties. In the case of the "$La_{0.7}Ca_{0.3}Mn_{1-x}Cu_xO_3$ + y SiO_2" samples, copper ions are trapped in the secondary phase and this leads to Mn site vacancies which have a stronger effect, the decrease of the transition temperature remaining much less pronounced than with Cu doping. When the ratio Si/Cu is too small, it appears that part of the copper ions remain in the manganate phase and are located preferentially near the grain boundaries : this is the cause of a double peak behaviour in the temperature dependence of the resistivity.

Acknowledgements

B.V. and Ph.V. are particularly grateful to the FNRS (Belgium) for fellowships. Part of this work has been financially supported by the Région Wallonne (Belgium).

References

[1]. K. Chahara, T. Ohno, M. Kasai and Y. Kozono, Appl. Phys. Lett. 63 (1993) 1990.
[2]. Y. Tokura, A. Urushibara, Y. Morimoto, T. Arima, A Asamitsu, G. Kidu and N. Furukawa, J. Phys. Soc. Jpn 63 (1994) 3931.
[3]. S. Jin, T.H. Tiefel, M. McCormack, R.A. Fastnacht, R. Ramesh and L.H. Chen, Science 264 (1994) 413.
[4]. G.A. Prinz, Phys. Today 4 (1995) 58.
[5]. C.N.R. Rao, A.K. Cheetham and R. Manesh, Chem. Mater. 8 (1996) 2421.
[6]. L.E. Gontchar, A.E. Nikiforov and S.E. Popov, J. Magn. Magn. Mater. 223 (2001) 1755.
[7]. D.I. Khomskii, cond-mat/0104517.
[8]. Y. Tomioka, T. Okuda, Y. Okimoto, A. Asamitsu, H. Kuwahara and Y. Tokura, J. Alloys Compd. 326 (2001) 27.
[9]. A. Maignan, C. Martin, G. Van Tendeloo, M. Hervieu and B. Raveau, Phys.Rev.B 60 (1999) 15214.
[10]. B. Raveau, M. Hervieu, A. Maignan and C. Martin, J. Mater. Chem. 11 (2001) 29.
[11]. C. Zener, Phys.Rev. 82 (1951) 403.
[12]. J.M.D. Coey, M. Viret and S. von Molnar, Adv. Phys. 48 (1999) 167.
[13]. R. Mahesh, R. Mahendiran, A.K. Raychaudhuri and C.N.R. Rao, J. Solid State Chem. 120 (1995) 204.
[14]. A. Maignan, C. Simon, V. Caignaert and B. Raveau, Z.Phys.B 99 (1996) 305.
[15]. A. Sundaresan, A. Maignan and B. Raveau, Phys.Rev.B 56 (1997) 5092.
[16]. L.M. Rodriguez-Martinez and J.P. Attfield, Phys.Rev.B 54 (1996) R15622.
[17]. K. Ghosh, S.B. Ogale, R. Ramesh, R.L. Greene, T. Venkatesan, K.M. Gapchup, R. Bathe and S.I. Patil, Phys.Rev.B 59 (1999) 533.

[18]. O. Cabeza, M. Long, C. Severac, M.A. Bari, C.M. Muirhead, M.G. Francesconi and C. Greaves, J. Phys. : Condens. Matter 11 (1999) 2569.
[19]. R. Ganguly, I.K. Gopalakrishnan and J.V. Yakhmi, Physica B 266 (1999) 332.
[20]. B. Raveau, C. Martin, A. Maignan, M. Hervieu and R. Mahendiran, Physica C 341-348 (2000) 711.
[21]. R. von Helmolt, L. Haupt, K. Bärner and U. Sondermann, Solid State Commun. 82 (1992) 693.
[22]. S.L. Yuan, Y. Jiang, G. Li, J.Q. Li, Y.P. Yang, X.Y. Zeng, P. Tang and Z. Huang, Phys.Rev.B 61 (2000) 3211.
[23]. K. Knizek, M. Daturi, G. Busca and C. Michel, J. Mater. Chem. 8 (1998) 1815.
[24]. Y. Sun, X. Xu, W. Tong and Y. Zhang, Appl. Phys. Lett. 77 (2000) 2734.
[25]. L. Pi, X. Xu and Y. Zhang, Phys.Rev.B 62 (2000) 5667.
[26]. K.Y. Wang, W.H. Song, J.M. Dai, S.L. Ye, S.G. Wang, J. Fang, J.L. Chen, B.J. Gao, J.J. Du and Y.P. Sun, J. Appl. Phys. 90 (2001) 6263.
[27]. C.L. Yuan, Y. Zhu and P.P. Ong, Solid State Commun. 120 (2001) 495.
[28]. S.L. Yuan, Z.Y. Li, X.Y. Zeng, G.Q. Zhang, F. Tu, G. Peng, J. Liu, Y. Jiang, Y.P. Yang and C.Q. Tang, Eur. Phys. J. B 20 (2001) 177.
[29]. T. Horita, J.S. Choi, Y.K. Lee, N. Sakai, T. Kawada, H. Yokokawa and M Dokiya, J. Am. Ceram. Soc. 78 (1995) 1729.
[30]. B. Dabrowski, R. Dybzinski, Z. Bukowski, O. Chmaissem and J.D. Jorgensen, J. Solid State Chem. 146 (1999) 448.
[31]. V. Verelst, N. Rangavittal, C.N.R. Rao and A. Rousset, J. Solid State Chem. 104 (1993) 74.
[32]. C. Ritter, M.R. Ibarra, J.M. De Teresa, P. Algarabel, C. Marquina, J. Blasco, J. Garcia, S. Oseroff and S.W.Cheong, Phys.Rev.B 56 (1997) 8902.
[33]. J. Chenavas, J.C. Joubert, M. Marezio and B. Bochu, J. Solid State Chem. 14 (1975) 25.
[34]. S.L. Yuan, Z.Y. Li, G.Q. Zhang, F. Tu, X.Y. Zeng, Y.P. Yang and C.Q. Tang, Solid State Commun. 117 (2001) 661.
[35]. C.H. Booth, F. Bridges, G.H. Kwei, J.M. Lawrence, A.L. Cornelius and J.J. Neumeier, Phys.Rev.B 57 (1998) 10440.
[36]. J.B. Goodenough, A. Wold, R.J. Arnott and N. Menyuk, Phys.Rev. 124 (1961) 373.
[37]. D. Khomskii, in : Spin Electronics, eds by M. Ziese and M.J. Thornton (Springer, Berlin, 2001), p. 89.
[38]. J. Töpfer and J.B. Goodenough, Chem. Mater. 9 (1997) 1467.
[39]. N. Zhang, F. Wang, W. Zhong and W. Ding, J. Phys.: Condens. Matter 11 (1999) 2625.
[40]. P.A. Joy, P.S. Anil Kumar and S.K. Date, Mater. Res. Bull. 34 (1999) 2143.
[41]. A.K.M. Akther Hossain, L.F. Cohen, T. Kodenkandeth, J. MacManus-Driscoll and N.McN. Alford, J Magn. Magn. Mater. 195 (1999) 31.
[42]. J.R. Sun, G.H. Rao and Y.Z. Zhang, Appl. Phys. Lett. 72 (1998) 3208.

Figure captions :

Fig.1 : X-ray patterns of the C4S0, C4S8 and C8S0 samples. Stars (*) indicate the reflections of the manganate phase, cross signs (+) indicate the reflections of the apatite-type phase.

Fig.2 : Temperature dependence of the electrical resistivity for the C2S0, C4S0 and C6S0 samples. Note that the resistivity of the C2S0 sample is multiplied by 10.

Fig.3 : Temperature dependence of the electrical resistivity for the C0S0, C0S4 and C0S8 samples.

Fig. 4 : Temperature dependence of the electrical resistivity for the C4S4 and C4S8 samples.

Fig. 5 : Temperature dependence of the electrical resistivity for the C4S2 and C8S4 samples.

Fig.6 : Temperature dependence of the AC in-phase magnetic moment of the C0S8, C4S8, C8S4 and C4S0 samples.

Fig.7 : Temperature dependence of the AC in-phase magnetic moment with superimposed DC fields for the C8S4 sample.

Fig.8 : Temperature dependence of the DC magnetic moment of the C8S4 sample for different DC magnetic fields.

Fig. 9 : Schematic representation of several possible virtual electron transfers in the Mn^{3+}, Mn^{4+}, Cu^{2+} system.

Label	Composition	T_p (K)	T_C (K)
C0S0	$La_{0.7}Ca_{0.3}MnO_3$	256.5	255
C0S4	$La_{0.7}Ca_{0.3}MnO_3$ + 0.04 SiO_2	255.5	252
C0S8	$La_{0.7}Ca_{0.3}MnO_3$ + 0.08 SiO_2	256	254
C2S0	$La_{0.7}Ca_{0.3}Mn_{0.98}Cu_{0.02}O_3$	248.5	246
C4S0	$La_{0.7}Ca_{0.3}Mn_{0.96}Cu_{0.04}O_3$	195	190
C6S0	$La_{0.7}Ca_{0.3}Mn_{0.94}Cu_{0.06}O_3$	158.5	152.5
C4S2	$La_{0.7}Ca_{0.3}Mn_{0.96}Cu_{0.04}O_3$ + 0.04 SiO_2	241.5 – 177	236
C4S4	$La_{0.7}Ca_{0.3}Mn_{0.96}Cu_{0.04}O_3$ + 0.04 SiO_2	245	242.5
C4S8	$La_{0.7}Ca_{0.3}Mn_{0.96}Cu_{0.04}O_3$ + 0.08 SiO_2	246	241.5
C8S4	$La_{0.7}Ca_{0.3}Mn_{0.92}Cu_{0.08}O_3$ + 0.04 SiO_2	229 – 146	218

Table 1 : Labels, compositions, resistive transition temperatures T_p and magnetic transition temperatures T_C

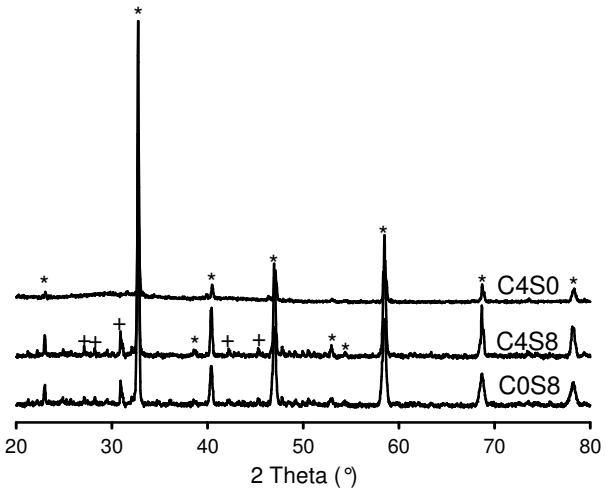

Figure 1

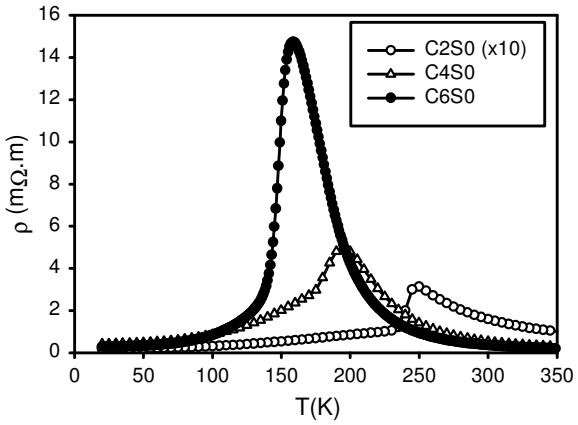
C2S0 (x10)
C4S0
C6S0
ρ (mΩ.m)
T(K)
0
2
4
6
8
10
12
14
16
0
50
100
150
200
250
300
350

Figure 2

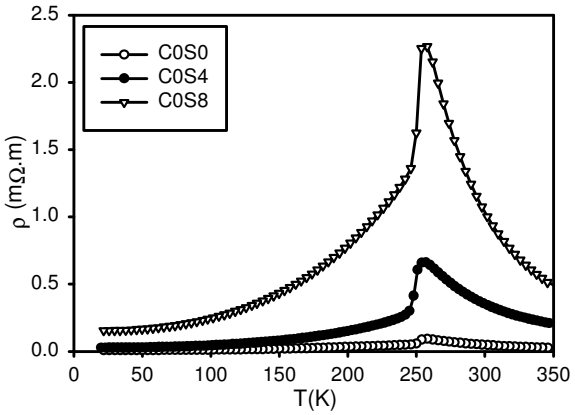
C0S0
C0S4
C0S8
ρ (mΩ.m)
T(K)
2.5
2.0
1.5
1.0
0.5
0.0
0
50
100
150
200
250
300
350

Figure 3

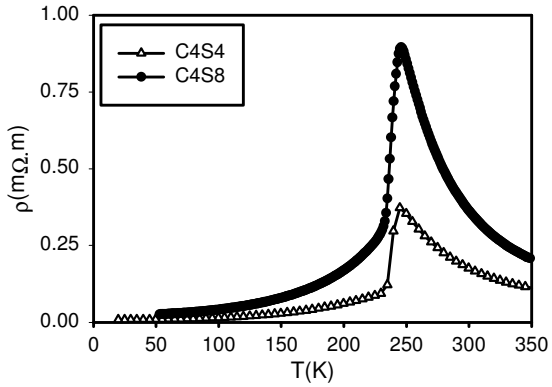
C4S4
C4S8
ρ(mΩ.m)
T(K)
1.00
0.75
0.50
0.25
0.00
0
50
100
150
200
250
300
350

Figure 4

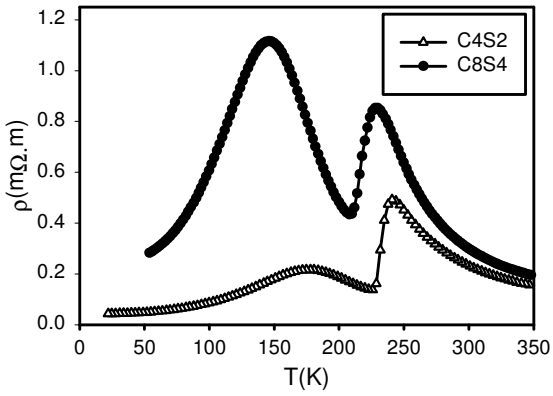

Figure 5

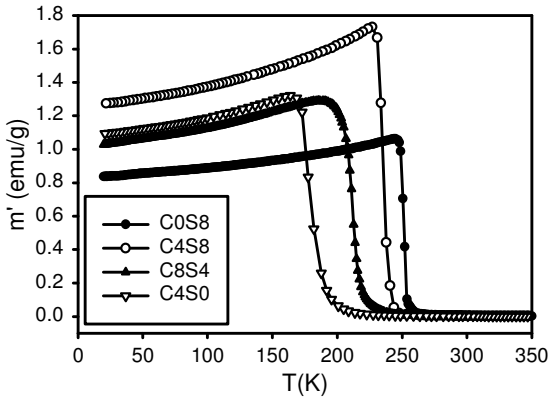
m' (emu/g)
T(K)
C0S8
C4S8
C8S4
C4S0
0.0
0.2
0.4
0.6
0.8
1.0
1.2
1.4
1.6
1.8
0
50
100
150
200
250
300
350

Figure 6

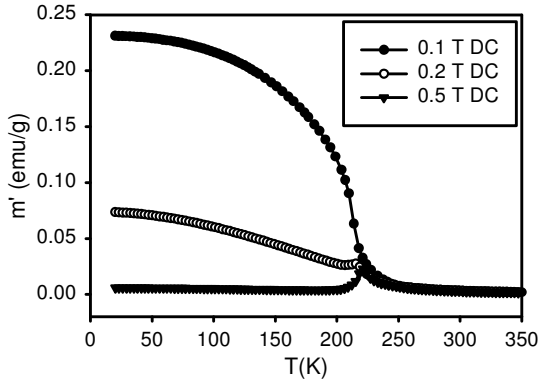
0.25
0.20
0.15
0.10
0.05
0.00
m' (emu/g)
0
50
100
150
200
250
300
350
T(K)
0.1 T DC
0.2 T DC
0.5 T DC

Figure 7

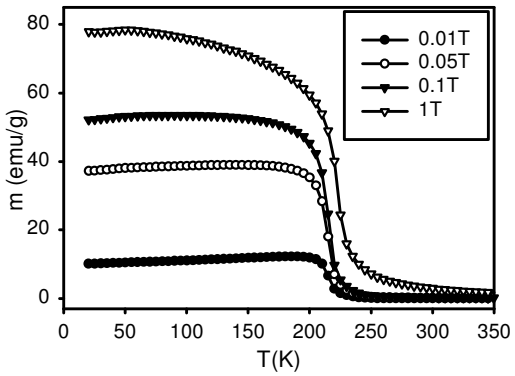
80
60
40
20
0
m (emu/g)
0
50
100
150
200
250
300
350
T(K)
0.01T
0.05T
0.1T
1T

Figure 8

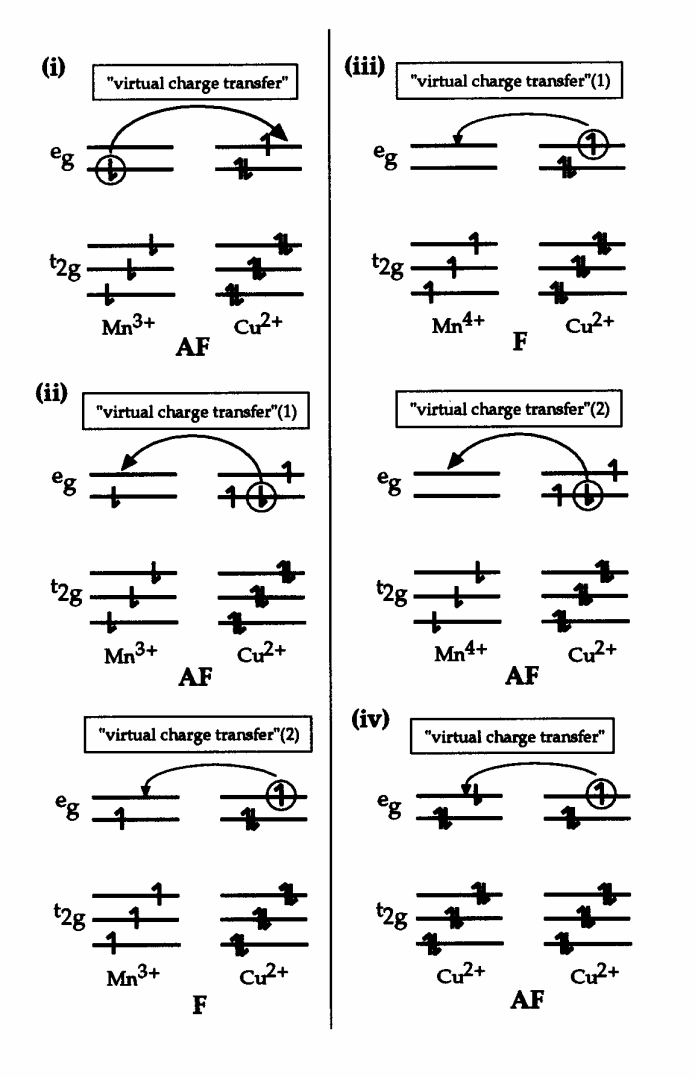
(i)
"virtual charge transfer"
eg
t2g
Mn3+
Cu2+
AF
(iii)
"virtual charge transfer"(1)
eg
t2g
Mn4+
Cu2+
F
(ii)
"virtual charge transfer"(1)
eg
t2g
Mn3+
Cu2+
AF
"virtual charge transfer"(2)
eg
t2g
Mn4+
Cu2+
AF
"virtual charge transfer"(2)
eg
t2g
Mn3+
Cu2+
F
(iv)
"virtual charge transfer"
eg
t2g
Cu2+
Cu2+
AF

Figure 9